Vacuum 145 (2017) 268–271

Contents lists available at ScienceDirect

Vacuum

journal homepage: www.elsevier.com/locate/vacuum

Short communication

Influence of the aluminum content on structure and optical properties of $Zr_{1-x}Al_xN$ films

Jian-ping Meng [a, b, *], Ke Zhang [c], Xiao-peng Liu [c], Zhi-qiang Fu [d], Zhou Li [a, b, **]

[a] Beijing Institute of Nanoenergy and Nanosystems, Chinese Academy of Sciences, Beijing 100083, China
[b] CAS Center for Excellence in Nanoscience, National Center for Nanoscience and Technology (NCNST), Beijing 100190, China
[c] Department of Energy Material and Technology, General Research Institute for Nonferrous Metals, Beijing 100088, China
[d] School of Engineering and Technology, China University of Geosciences (Beijing), Beijing 100083, China

ARTICLE INFO

Article history:
Received 4 May 2017
Received in revised form
3 August 2017
Accepted 5 August 2017
Available online 8 September 2017

Keywords:
Ion beam assisted deposited
Aluminum content
$Zr_{1-x}Al_xN$ films
Electrical resistivity
Optical constants

ABSTRACT

The $Zr_{1-x}Al_xN$ films have been deposited on Si (111) and glass (soda lime glass) substrates by ion beam assisted deposition. The microstructure, morphology, electrical resistivity and optical properties of the $Zr_{1-x}Al_xN$ films were investigated by XRD, TEM, four-probe method and spectroscopic ellipsometry. In the Al composition range $0.32 \leq x \leq 0.7$, the $Zr_{1-x}Al_xN$ films contain crystallized ZrAlN (NaCl type). The deposited $Zr_{0.2}Al_{0.8}N$ film is amorphous. The aluminum content increase in the $Zr_{1-x}Al_xN$ films induces the film structure tends to amorphization. The refractive index of the $Zr_{1-x}Al_xN$ films increases with Al content increase, whereas, a continuous decrease of the extinction coefficient was noticed. As the Al content increase, the electrical resistivity of films increases. The addition of Al into ZrN-based films leads to the loss of the metallic character.

ZrN is one of the nitrides of the group IVB transition metals (titanium, zirconium and hafnium). It combines high mechanica1 hardness, high melt point and high corrosion resistance with high electrical and thermal conductivity [1–3]. The underlying cause for these properties is special bonding structure which is a combination of ionic, metallic, and valence bonding between *pd* hybrids [4]. Whereas, the microstructure and properties of ZrN films need to be modified or decorated according to the application. Indeed, the introduction of a third element into transition metal nitride coatings is a significant way to modify their microstructure and properties. Incorporation of Al atoms to transition metal nitride films can progressively modify the crystallite orientation, improves the resistance against oxidation and also increases significantly the hardness of the films. It has been reported that ZrAlN films change their crystal structures by the incorporation of Al atoms [5–8]. Moreover, the oxidation resistance of Zr–Al–N films is also improved due to the formation of successive and compact Al_2O_3 phase, which hinders oxygen to diffuse into the inner coatings under high temperature environment [9]. Additionally, the physical properties of the ZrN are linked to their electronic structure, the replacement in the lattice of Zr atoms by Al atoms induces the changes in the bonding formation with several consequences [10]. The important effects are a decrease of the free carrier concentration, significant local modifications of the covalent–ionic bonding involving the N 2p and Zr 4d orbitals, and the lattice shrinkage. In this work, a detailed experimental investigation is reported of the structural, electrical, and optical properties of $Zr_{1-x}Al_xN$ thin films with $0.32 \leq x \leq 0.8$.

$Zr_{1-x}Al_xN$ films were deposited on single crystal Si (111) and glass (soda lime glass) substrates by ion beam assisted deposition (Type: ISB700). Prior to the depositions, the substrates were ultrasonically cleaned in acetone and ethanol for 10 min, respectively. When the base pressure was evacuated up to 2.0×10^{-4} Pa, the Zr (99.9% purity) and Al (99.999% purity) targets were etched by Ar ion generated by Kauffman ion source. Then, the substrate was etched by Ar ion with the energy of 800 eV. During the deposition, The Zr and Al targets were sputtered by argon ion generated by Kauffman ion source. The incident angle of the argon ion is 45°. The assisted nitrogen atoms with the incident angle of 45° bombarded the

* Corresponding author. Beijing Institute of Nanoenergy and Nanosystems, Chinese Academy of Sciences, Beijing 100083, China.
** Corresponding author. Beijing Institute of Nanoenergy and Nanosystems, Chinese Academy of Sciences, Beijing 100083, China.
E-mail addresses: mengjianpingallgood@gmail.com (J.-p. Meng), zli@binn.cas.cn (Z. Li).

http://dx.doi.org/10.1016/j.vacuum.2017.08.045
0042-207X/

substrate to synthesize the $Zr_{1-x}Al_xN$ during the Zr and Al atoms arriving at substrate. The substrate was rotated to ensure a uniform deposition. The substrate temperature was the room temperature. The aluminum content in the $Zr_{1-x}Al_xN$ films is controlled by adjusting the supplying ion beam current of the sputtering ion source applied on Al and Zr target. The deposition time was 30 min. The detail deposition parameter of $Zr_xAl_{1-x}N$ films was listed in Table 1.

The phase structure was determined by using X-ray diffraction (XRD, D/max-RB, Cu Kα) with the grazing incidence angle fixed at 1.0°. The scanning speed is 4°/min. A Tecnai G^2 F20 transmission electron microscope was used to investigate the film microstructure. The electrical resistivity was measured by using a four-probe method at room temperature. Spectroscopic ellipsometry (M-2000UI) was used to determine the optical constants. The incidence angle was fixed at 70°.

The XRD patterns of $Zr_{1-x}Al_xN$ films prepared at the different Al concentration are shown in Fig. 1. In the case of the Al content in the composition range from 0.32 to 0.7, all the diffraction peaks pertain to lattice plains of ZrN phase (NaCl-type structure). In addition, the position of the X-ray diffraction peaks monotonously shifts towards the higher diffraction angles with the increase of Al content in the films. This indicates the lattice constant of the $Zr_{1-x}Al_xN$ films decreases with the increase of Al content. This phenomenon is due to the substitution of zirconium atoms by aluminum atoms which has the smaller atom radius than the atom radius of zirconium. Additionally, as the aluminum content increases in the $Zr_{1-x}Al_xN$ films, the diffraction peak intensity is weaken. For the $Zr_{0.2}A_{0.8}N$ film, no diffraction peaks are observed, which indicates the deposited film is amorphous.

Fig. 2 shows the cross-section, SAED and HRTEM images of the $Zr_{0.6}Al_{0.4}N$ (a) and $Zr_{0.4}Al_{0.6}N$ (b) films. From the cross-section image of the $Zr_{0.6}Al_{0.4}N$ film (see Fig. 2a), the film displays columnar structure. The interplanar distances measured from the diffraction role (SAED image) match to the *c*-ZrAlN (PDF database file 02-0956). The diffraction patterns are indexed as (111), (200), (220), (311) and (222) reflections, indicating the polycrystalline state. The only crystalline phase of *c*-ZrAlN can be observed in the HRTEM image of the $Zr_{0.6}Al_{0.4}N$ film. Additionally, a little of amorphous phase can also be noted. Fig. 2b shows the cross-section, SAED and HRTEM images of the $Zr_{0.4}Al_{0.6}N$ film. The columnar crystal (dark area) and amorphous around it is notable. This phenomenon can also be confirmed from the HRTEM image. The diffraction role of the $Zr_{0.4}Al_{0.6}N$ film is ascribe to the panels of (111), (200) (220) and (311) of *c*-ZrAlN. The diffraction role of the $Zr_{0.6}Al_{0.4}N$ films is more sharp and brighter than the diffraction role of $Zr_{0.4}Al_{0.6}N$. Those results indicate that the content of crystalline phase in the $Zr_{0.6}Al_{0.4}N$ film is more than it in the $Zr_{0.4}Al_{0.6}N$ film. This results are in accord with the XRD results.

Table 1
The deposition parameter of $Zr_xAl_{1-x}N$ films.

$Zr_xAl_{1-x}N$	Sputtering ion source (Zr target)		Sputtering ion source (Al target)		Assisted ion source	
	Ar = 5.00 SCCM		Ar = 5.00 SCCM		N_2 = 6.00 SCCM	
	AIE (eV)	AIC (mA)	AIE (eV)	AIC(mA)	ASIE (eV)	ASIC (mA)
$Zr_{0.68}Al_{0.32}N$	2700	120	2700	80	200	50
$Zr_{0.6}Al_{0.4}N$	2700	120	2700	100	200	50
$Zr_{0.5}Al_{0.5}N$	2700	100	2700	100	200	50
$Zr_{0.4}Al_{0.6}N$	2700	80	2700	100	200	50
$Zr_{0.3}Al_{0.7}N$	2700	60	2700	100	200	50
$Zr_{0.2}Al_{0.8}N$	2700	40	2700	100	200	50

AIE, AIC, ASIE, and ASIC correspond to argon ion energy, argon ion current, assisted ion energy and assisted ion current.

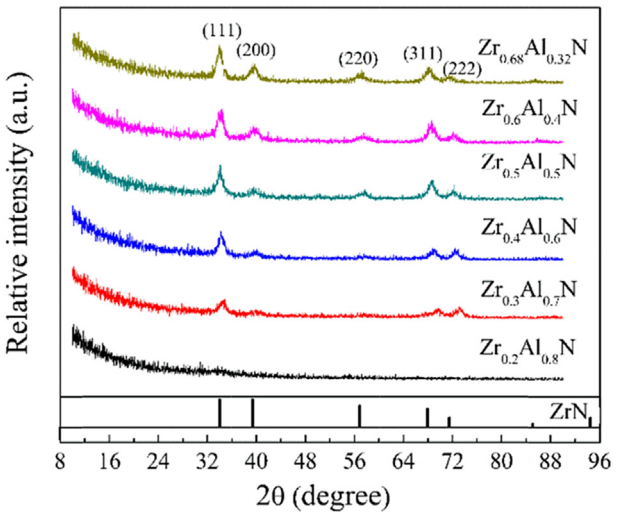

Fig. 1. XRD pattern of $Zr_{1-x}Al_xN$ films deposited at different at different Al concentrations x.

The aluminum content increase in the $Zr_{1-x}Al_xN$ films induces the increase of the lattice shrinkage and distortions [11,12], which increases the defect and amorphous phase in the films. Additionally, for $x \leq 0.472$, the $Zr_{1-x}Al_xN$ solid solution is stable in *fcc* structure (NaCl type). Beyond this composition in the films, the poorly crystallized AlN phase may form in the deposited films [12]. Those factors induce the diffraction peak is weakened. When Al content is 0.8, the crystallized phase is too little to reach the detectable limit of XRD. The XRD results display the $Zr_{0.2}Al_{0.8}N$ films is amorphous.

The electrical resistivity of $Zr_{1-x}Al_xN$ films is shown in Fig. 3. As the Al content increase in the films, the electrical resistivity increases. When the Al content increases from 0.32 to 0.5, the electrical resistivity increases from 184 μΩ•cm to 302 μΩ•cm, indistinctively. The electrical resistivity increases to 976 μΩ•cm dramatically as the Al content increases from 0.5 to 0.6. The electrical resistivity of the $Zr_{0.2}Al_{0.8}$ films reaches to 47107 μΩ•cm. In addition to the instinct property of materials, the total resistivity is a contribution of several independent electron scattering process due to the phonons, impurity atom and defect. ZrN exhibits metallic property, such as low resistivity and high absorption for the visible and infrared region due to the combination of ionic, metallic, and valence bonding between *pd* hybrids [4]. For $0.32 \leq x \leq 0.5$, the Al atoms substitute Zr atoms in the ZrN lattice The substitution of Zr^{4+} by Al^{3+} ions in the subcationic lattice reduces the charge carriers density near the Fermi level (Al does not have d electrons), which decreases the free electrons density [10]. The electrical resistivity increases. The increase of aluminum content in the films leads to the shrinkage of the cell and amorphization, which means the high presence of defects. It reinforces the electron scattering effect. Additionally, the new phases of *h*-AlZrN (Al-rich, wurtzite-type) and *h*-AlN may form in the films [11–14]. *h*-AlZrN is a poorly conductive phase, and *h*-AlN is a semiconductor. The presence of *h*-AlZrN and *h*-AlN leads to the decrease of the lifetime of the free electrons. The electrical resistivity of films increases, further [15].

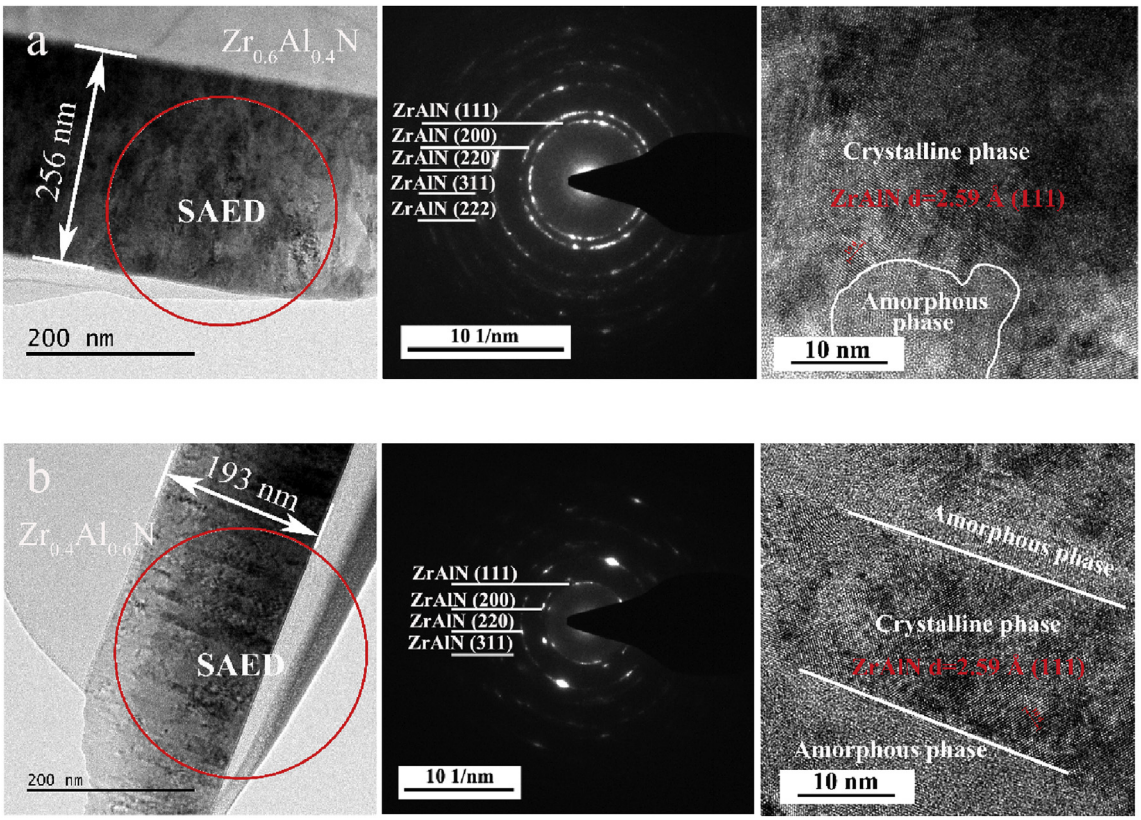

Fig. 2. Cross-section, SAED and HRTEM images of the $Zr_{0.6}Al_{0.4}N$ (a) and $Zr_{0.4}Al_{0.6}N$ (b) films.

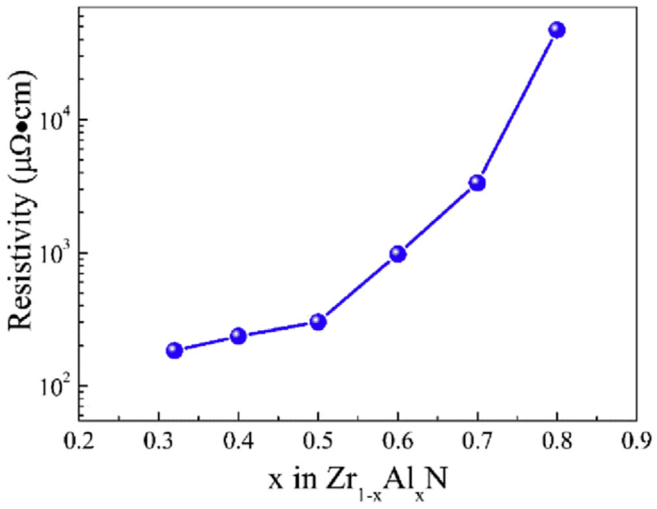

Fig. 3. Electrical resistivity of $Zr_{1-x}Al_xN$ films as a function of x.

The optical constants of $Zr_{1-x}Al_xN$ films are shown in Fig. 4. As the Al content increases from 0.32 to 0.70, the refractive index increases on the whole spectral range, whereas, the extinction coefficient decreases. For $0.32 \leq x \leq 0.7$, the refractive index of the deposited $Zr_{1-x}Al_xN$ films decreases in the wavelength range from 250 nm to 500 nm, then, increases with the wavelength increase. The extinction coefficient decrease in the wavelength range between 250 and 380 nm, then, increases. The extinction coefficient displays high absorption in the infrared radiation range due to the free electron and lower absorption in the ultraviolet-visible range. Additionally, the slope of extinction coefficient is highly lowered. Increase the Al content in the films, the Al-N bond increases in the films. It will decrease the free electron density or their mobility. It is confirmed from the electrical resistivity results. For $Zr_{0.2}Al_{0.8}N$ films, the refractive index and extinction coefficient decrease as the wavelength increase. The extinction coefficient value is between 0.2 and 0.5, indicating the dielectric behavior. From the results of electrical resistivity and optical constants, as the Al content increases in the $Zr_{1-x}Al_xN$ films, the metallic behavior is weakened, whereas, the dielectric behavior is reinforced.

The $Zr_{1-x}Al_xN$ films are successfully deposited on silicon and glass (soda lime glass) substrates by ion beam assisted deposition. The effect of Al content on the film structure, electrical resistivity and optical properties is studied. In the Al composition range $0.32 \leq x \leq 0.7$, the deposited $Zr_{1-x}Al_xN$ films contain crystallized ZrAlN (NaCl type). The deposited $Zr_{0.2}Al_{0.8}N$ film is amorphous. The aluminum content increase in the $Zr_{1-x}Al_xN$ films induces the film structure tends to amorphization. As the Al content increases, the electrical resistivity increases. The refractive index increases with the Al content increase, whereas, the extinction coefficient decreases. Thus, addition of Al into ZrN-based films leads to the loss of the metallic character.

This work was supported by Program of China (Grant No. 2015BAA02B04) under the Ministry of Science and Technology of China, NSFC (31571006) and “Thousands Talents” program for

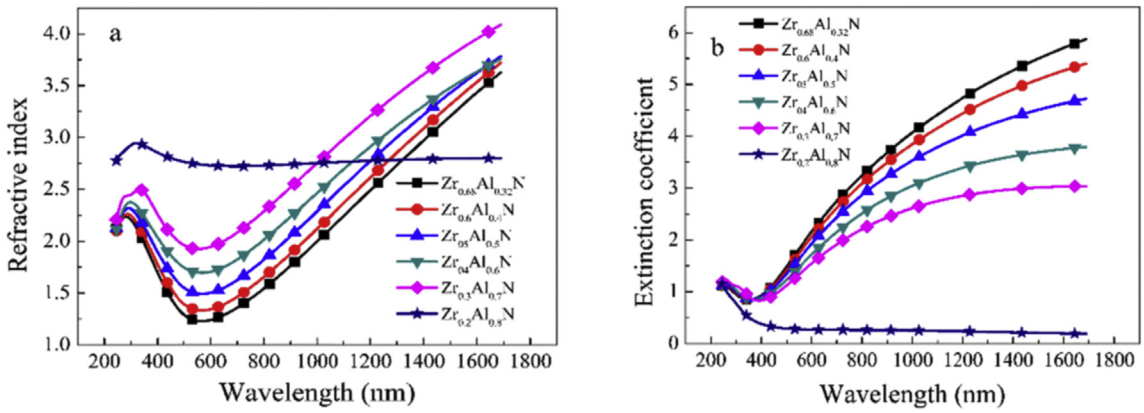

Fig. 4. Optical constants of $Zr_{1-x}Al_xN$ films as a function of x.

pioneer researcher and his innovation team.

References

[1] C.P. Liu, H.G. Yang, Deposition temperature and thickness effects on the characteristics of dc-sputtered ZrN_x films, Mater. Chem. Phys. 86 (2004) 370–374.

[2] J.J. Araiza, O. Sánchez, J.M. Albella, Influence of the aluminum incorporation on the structure of sputtered ZrNx films deposited at low temperatures, Vacuum 83 (2009) 1236–1239.

[3] J.P. Meng, Z.Q. Fu, M. Du, X.P. Liu, L. Hao, Influence of ion–atom arrival ratio on structure and optical properties of ZrN_x films, Mater. Lett. 164 (2016) 291–293.

[4] M. Veszelei, K. Andersson, C.G. Ribbing, K. Jarrendahl, H. Arwin, Optical constants and Drude analysis of sputtered zirconium nitride films, Appl. Opt. 33 (1994) 1993–2001.

[5] P.H. Mayrhofer, D. Sonnleitner, M. Bartosik, D. Holec, Structural and mechanical evolution of reactively and non-reactively sputtered Zr–Al–N thin films during annealing, Surf. Coat. Technol. 244 (2014) 52–56.

[6] L. Rogström, M.P. Johansson-Jõesaar, L. Landälv, M. Ahlgren, M. Odén, Wear behavior of ZrAlN coated cutting tools during turning, Surf. Coat. Technol. 282 (2015) 180–187.

[7] G. Abadias, I.A. Saladukhin, V.V. Uglov, S.V. Zlotski, D. Eyidi, Thermal stability and oxidation behavior of quaternary TiZrAlN agnetron sputtered thin films: influence of the pristine microstructure, Surf. Coat. Technol. 237 (2013) 187–195.

[8] R. Franz, M. Lechthaler, C. Polzer, C. Mitterer, Oxidation behaviour and tribological properties of arc-evaporated ZrAlN hard coatings, Surf. Coat. Technol. 206 (2012) 2337–2345.

[9] G. Xian, H.B. Zhao, H.Y. Fan, H. Wang, H. Du, The structure and properties of ZrAl(Y)N coatings deposited at various N_2/Ar flow ratios, Int. J. Refract. Met. Hard Mater 44 (2014) 60–67.

[10] R. Lamni, R. Sanjinés, F. Lévy, Electrical and optical properties of $Zr_{1-x}Al_xN$ thin films, Thin Solid Films 478 (2005) 170–175.

[11] D. Holec, R. Rachbauer, L. Chen, L. Wan, D. Luef, P.H. Mayrhofer, Phase stability and alloy-related trends in Ti–Al–N, Zr–Al–N and Hf–Al–N systems from first principles, Surf. Coat. Technol. 206 (2011) 1698–1704.

[12] S.H. Sheng, R.F. Zhang, S. Veprek, Phase stabilities and thermal decomposition in the $Zr_{1-x}Al_xN$ system studied by ab initio calculation and thermodynamic modeling, Acta Mater 56 (2008) 968–976.

[13] E.D. Gutiérrez-Senior, J. Sierra-Ortega, Structural and electronic properties of $Zr_xAl_{1-x}N$ in cubic phase using first principles, J. Supercond. Nov. Magn. 26 (2013) 2471–2473.

[14] P.H. Mayrhofer, D. Music, J.M. Schneider, Influence of the Al distribution on the structure, elastic properties, and phase stability of supersaturated $Ti_{1-x}Al_xN$, J. Appl. Phys. 100 (2006) 094906.

[15] D. Pilloud, J.F. Pierson, L. Pichon, Influence of the silicon concentration on the optical and electrical properties of reactively sputtered Zr–Si–N nanocomposite coatings, Mater. Sci. Eng. B 131 (2006) 36–39.